Journal of Power Sources 196 (2011) 7816–7822

Contents lists available at ScienceDirect

Journal of Power Sources

journal homepage: www.elsevier.com/locate/jpowsour

High-frequency carbon supercapacitors from polyfurfuryl alcohol

V. Ruiz*, A.G. Pandolfo

CSIRO Division of Energy Technology, Box 312, Clayton South, Vic. 3169, Australia

ARTICLE INFO

Article history:
Received 20 September 2010
Received in revised form
10 December 2010
Accepted 13 December 2010
Available online 19 January 2011

Keywords:
Electrical double-layer capacitors
High-frequency performance
Electrochemical properties
Polyfurfuryl alcohol
Rate capability

ABSTRACT

Porous carbons with controllable and narrow pore-size distributions are prepared from the chemical activation of polyfurfuryl alcohol (PFA). High *apparent* BET surface areas, up to 2600 $m^2 g^{-1}$ (2611 $m^2 g^{-1}$ by Density Functional Theory (DFT)), and good electrical conductivities (up to ~130 $S cm^{-1}$) are obtained. By varying the potassium hydroxide: carbon precursor ratio, the preparation of carbons with different proportions of micro- and fine mesoporosity (<5 nm) can be tailored to provide an ideal electronic and ionic pore structure for electrochemical energy-storage devices, such as electrical double-layer capacitors. High specific capacitance values are obtained up to 147 $F g^{-1}$ in a voltage window of 2.5 V using 1 M tetraethyl ammonium tetrafluoroborate in acetonitrile. Moreover, excellent high-current and high-frequency performance is demonstrated: 100 $F g^{-1}$ at 225 $A g^{-1}$ (10 Hz) and ~30 $F g^{-1}$ at 100 Hz. When comparing the performance with commercial activated carbons (ACs) of similar textural properties, the PFA-derived ACs demonstrated better performance in terms of higher capacitance values and improved rate capabilities. There is a 125% increase in capacitance values at 1 kHz.

1. Introduction

Electrical double-layer capacitors, EDLCs (also known as supercapacitors or ultracapacitors) are complementary energy-storage devices to batteries [1–3]. They combine higher specific power than conventional batteries and higher specific energy than conventional capacitors, along with longer cycle-life and environmental friendliness. EDLCs are finding niche applications where their greater reliability, lifetime and power delivery are preferred over the higher specific energy of batteries (e.g., portable devices, consumer electronics, industrial power management, hybrid vehicles, power back-up and quality systems [4–6]).

While EDLCs contain far greater energy than conventional capacitors, most of the capacitance resides at the surface of fine pores that are accessed over relatively long time scales (~seconds *c.f.* < 10^{-6} s for conventional capacitors). Therefore, the frequency response of EDLCs is poor and energy can only be withdrawn at relatively low frequencies. For many applications, the low frequency response of EDLCs can be adequately accommodated. There is, however a growing need for EDLCs that can act as replacements for the numerous and bulky arrays of conventional capacitors used as voltage regulators in electronic devices. Typical applications that would benefit from this are: pagers, personal data assistance devices, notebooks, and cell phones. EDLCs used in these devices require a very low resistance and a high capacitance at d.c. levels; but also need to be designed to deliver power at higher frequencies.

The capacitance in an EDLC is stored at the double layer formed at the carbon surface–electrolyte interface. Although the surface area of the carbon material plays an important role in the double layer formation, its pore-size distribution and the molecular dimensions of the electrolyte ions [7] can be crucial. In active carbons (ACs) most of the surface area resides in small micropores which, depending on the size of the electrolyte ions, might be physically incapable of supporting an electrical double layer; thus resulting in a reduced or poor high-frequency response. Therefore, the optimization of carbon pore size, while maintaining a high surface area, is critical for the development of EDLCs with improved high-frequency characteristics.

Commonly, high surface area carbon materials (e.g., ACs) are used in conventional EDLCs [2,8]. They are typically derived from coal, anthracites, petroleum cokes, lignocellulosic materials [9–11] or synthetic carbon precursors, and are generally polymeric in nature [12–15]. Preparation techniques involve traditional activation methods (e.g., physical activation, chemical activation, or a combination of both [16–18]).

This study concerns the preparation and characterization of conductive carbons, with characteristically narrow and controllable pore-size distributions, from furfuryl alcohol (FA), which is a low-cost precursor that can be sourced from agricultural waste [19]. The use of synthetic carbon precursors offers several advantages over traditional precursors such as homogeneity of feed and the absence of inorganic impurities. Despite a limited number of published studies on the physical activation of PFA and subsequent testing as active materials in supercapacitors [5,20], no electrochemical studies on ACs derived from the chemical activation of PFA have been reported. A detailed evaluation of the properties

* Corresponding author. Tel.: +61 3954 58648; fax: +61 39562 8919.
E-mail addresses: vanesa.ruizruiz@csiro.au, vanesarz79@gmail.com (V. Ruiz).

0378-7753/$ – see front matter © 2011 Published by Elsevier B.V.
doi:10.1016/j.jpowsour.2010.12.111

and electrochemical performance of ACs derived from PFA as electrode materials for EDLCs is presented and their high-frequency performance is compared with commercial ACs.

2. Experimental

2.1. Materials

The synthesis of PFA has been described elsewhere [20]. Resins derived from furfuryl alcohol (FA) undergo polycondensation under the action of an acidic catalyst which leads to a highly cross-linked black viscous product [21]. The resultant polymer was chemically activated by using KOH as activating agent. PFA was mixed with potassium hydroxide in proportions of: 1:1, 2:1, 2.5:1 or 3:1 KOH: PFA-precursor. The mixture was then placed in a crucible and heated at 700 °C for 1 h, under a nitrogen flow (90 ml min^{-1}). The system was allowed to cool to room temperature and the product was neutralized with HCl (1 h reflux) and thoroughly washed with distilled water until pH = 7. The resultant activated carbons were labelled PFA-K*X*, where *X* refers to the amount of chemical agent used.

Several commercial ACs were evaluated for comparison purposes. Maxsorb®, DLC-Supra and RP-20 ACs were supplied by Kansai Coke and Chemicals Co., Ltd., Kuraray Chemical Co. Ltd. and Norit Americas Ltd., respectively.

2.2. Material characterization—surface area and pore analysis

Physical adsorption of nitrogen at 77 K and carbon dioxide at 273 K was performed by means of a *Micromeritics ASAP* 2010 analyser. The apparent specific BET surface area was determined from the N_2-adsorption isotherm. The total pore volume (TPV) was obtained from the N_2 isotherm at a relative pressure $P/P_0 = 0.99$ and the volume of mesopores (V_{meso}) was estimated by subtracting the volume of micropores (V_m) calculated by applying the Dubinin–Radushkevich (D–R) equation from TPV. The micropore surface area (S_{mic}) was obtained from application of the D–R equation to the N_2 isotherm [22]. The pore-size distributions were estimated by DFT analysis assuming slit shape pores. The average micropore width, L_0, was calculated using $L_0 = 10.8/(E_0 - 11.4)$ nm [23], where E_0 is the characteristic energy (the structural constant *B* of the D–R equation).

The electrical conductivity of compacted powdered carbons was determined using a GW Milli-ohm meter GOM-801G, equipped with a four-point probe [24].

The oxygen content of the activated carbons was determined by direct determination using a LECOTF-900 furnace coupled to a LECO-CHNS-932 microanalyser.

2.3. Electrode preparation and electrochemical testing

Two-electrode test cells were assembled in order to evaluate the performance of the ACs. Electrochemical cells were sealed in laminated pouches and carbon coated on aluminium collectors (2.5 × 2.5 cm) served as electrodes. The composition of the carbon coating was: AC, carbon black and carboxymethylcellulose (CMC) binder in proportions of 1:0.2:0.1 with the minimum amount of water necessary to form a slurry. The carbon mixture was coated on aluminium foil with a 36 μm grooved rod applicator and the electrodes were thoroughly dried before assembly in a nitrogen-filled dry box. A 25 μm polypropylene separator was used as a separator and a solution of 1 M tetraethyl ammonium tetrafluoroborate in acetonitrile (Et_4NBF_4/ACN) as electrolyte.

Electrochemical testing was performed with a *Solatron* 1255B electrochemical analyser equipped with a 1470 multi-channel battery test module. Galvanostatic cycling of the supercapacitors was carried out between 0 and 2.5 V at current densities that ranged from 0.30 to 225 A g^{-1} (based on the weight of the active material of one electrode). The capacitance of the cell was obtained by applying the following equation: $C_{capacitor}$ (F) = $I/(dV/dt)$ to the constant-current discharge curve (avoiding the ohmic drop). Electrochemical impedance spectroscopy measurements were undertaken in order to study the resistance of the carbon electrodes in the frequency range: 10 mHz to 100 kHz with an a.c. amplitude of 10 mV. All impedance measurements were performed at open-circuit potential (OCP) on completely discharged cells.

3. Results and discussion

3.1. Pore-structure and properties of PFA-derived samples

Chemical activation of PFA leads to the formation of highly microporous activated carbons displaying distinctive type I isotherms (Fig. 1(a)). For a KOH to PFA ratio of 1:1, a highly microporous material is obtained (sample PFA-K1) with an apparent BET surface area of 1070 m^2 g^{-1} and a very narrow, and uniform, average micropore size, viz., $L_0 \sim 0.6$ nm (Table 1). The corresponding DFT pore size curve for the PFA-K1 sample (Fig. 1(b)) confirms the presence of very fine pores and also demonstrates the pore size uniformity of this sample with ~95% of its porosity attributed to pores of ~0.6 nm.

An increase in the amount of chemical agent leads to a broadening of the knee in the N_2-adsorption isotherms at low relative pressures (Fig. 1(a)) and a corresponding increase in both the surface area and the average micropore size (Table 1). Additional microporosity is formed together with an accompanying increase in fine mesoporosity that most likely arises from an enlargement of existing smaller pores [25,26]. The DFT pore size profiles of the ACs (Fig. 1(b)) display a gradual increase in average pore size with increasing degree of activation. The average micropore size (L_0) increases from 0.6 nm for the PFA-K1 sample to 1.6 nm for the PFA-K3 sample (Table 1). When the KOH:PFA ratio is 3:1, the proportion of microporosity begins to decline and a large amount of additional fine mesoporosity (<~5 nm) develops. Sample PFA-K3 has micropore and mesopore volumes of 0.93 and 0.73 cm^3 g^{-1}, respectively. Despite its high proportion of mesoporosity, which often leads to reduced surface areas, PFA-K3 still has a desirably high surface area ($S_{BET} \approx 2600$ m^2 g^{-1}).

The electrical resistivity of the PFA-derived carbons was also measured and the results are summarized in Fig. 2. A decrease in resistivity (increase in conductivity) of the tested carbon samples is observed when the applied pressure is increased (the compression of individual particles in the composite material will create more dense packing and closer contacts between them [27,28]), but quantifiable differences can be identified at a similar compaction pressures. Despite the moderately low activation temperature employed (700 °C), relatively low resistivity (high conductivity) values were obtained (Fig. 2). Sample PFA-K1 has a low resistivity, 0.041 Ω cm at 36 MPa (corresponds to a conductivity of 130 S cm^{-1}), but the resistivity increases with further activation. This trend is attributed to the presence of fewer conductive pathways (increased porosity, lower skeletal density) and greater structural disorder in agreement with similar studies [29–33]. Moreover, the increase in oxygen content with the degree of activation (from a 3.11 wt.% for a 1:1 PFA to KOH ratio to 7.62 wt.% when the ratio is 3:1, Table 1) has a negative effect of the electrical conductivity of the ACs [8,34]. This is because the higher the oxygen content, the greater is the barrier for electrons to move through the carbonaceous structure [35–37].

Despite the excellent conductivity of the PFA carbons, carbon black has also been incorporated into the electrode as

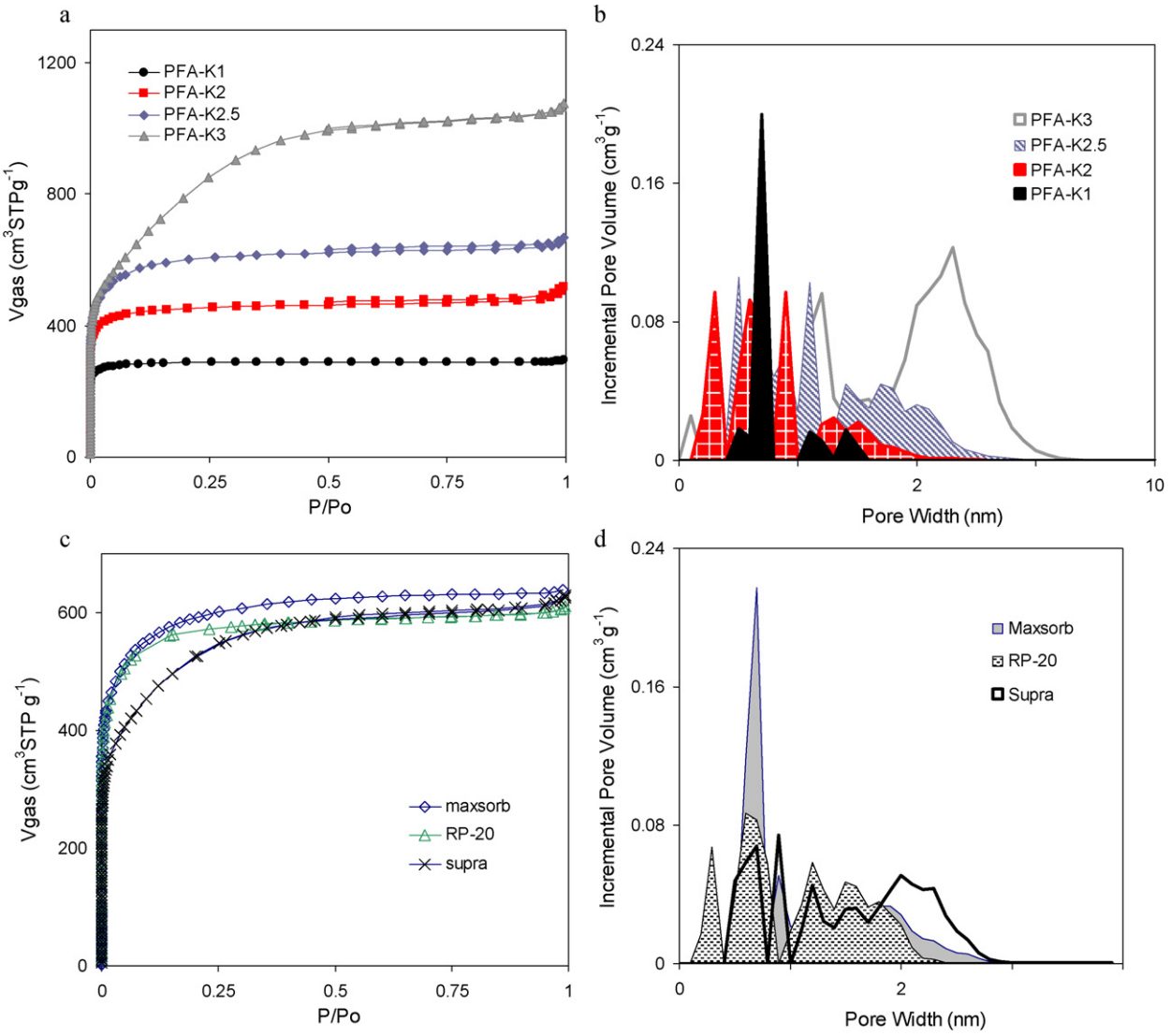

Fig. 1. N_2/77 K adsorption isotherms and DFT pore-size distribution for the PFA-series (a and b) and commercial samples (c and d).

its use in electrode preparation has been shown to reduce the inter-particle contact resistance for powdered ACs, particularly for electrodes fabricated with little or no compaction pressure [38].

3.2. Electrochemical properties of PFA-derived samples

Galvanostatic cycling of electrochemical devices containing the PFA carbons, at several current densities, was used to calculate the specific capacitance values displayed in Table 2; the current density was varied from 0.3 to 225 A g^{-1}. The highest capacitance values are obtained at low current density and then the values decrease as the current density increases. For some samples, this effect is quite rapid as in the case of sample PFA-K1 and the behaviour can be explained by the small pore size of this material. With only an average pore size of 0.6 nm (L_0 value in Table 1) accessibility issues regarding the movement of electrolyte ions into the pores can be expected. This was experimentally confirmed by performing cyclic voltammetry experiments in a three-electrode configuration where 'ion sieving' issues were clearly visible (data published in

Table 1
Characteristics of porous carbon materials prepared from PFA.

Sample	S_{BET} [$m^2 g^{-1}$]	S_{DFT} [$m^2 g^{-1}$]	S_{mic} [$m^2 g^{-1}$]	L_0 [nm]	V_{meso} [$cm^3 g^{-1}$]	V_m [$cm^3 g^{-1}$]	TPV [$cm^3 g^{-1}$]	Micropore content [%]	O (wt.%)
PFA-K1	1070	938	1448	0.6	0.03	0.43	0.46	95	3.11
PFA-K2	1600	1440	1696	0.8	0.13	0.67	0.80	84	4.6
PFA-K2.5	2180	1875	2423	1.0	0.21	0.82	1.03	80	4.36
PFA-K3	2600	2611	1145	1.6	0.73	0.93	1.66	56	7.62
Maxsorb	2112	2142	1513	1.05	0.24	0.79	1.04	80	n.a.
RP-20	2000	1815	757	1.12	0.16	0.78	0.94	83	n.a.
Supra	1872	1730	825	1.26	0.34	0.63	0.97	65	n.a.

S_{BET}, apparent BET area; S_{DFT}, DFT surface area; S_{mic}, microporous surface area from D–R equation, L_0, average micropore diameter; V_{meso}, volume of mesopores; V_m, volume of micropores determined from N_2 isotherm; TPV, total pore volume; k, bulk electrical conductivity.

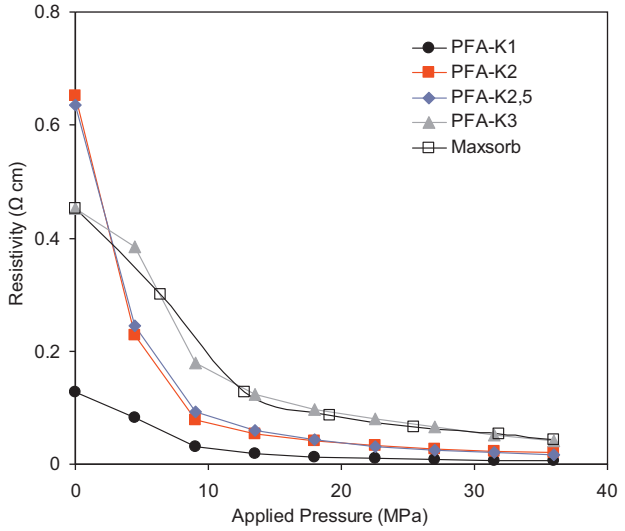

Fig. 2. Variation in electrical resistivity of powdered activated carbons under increasing compaction pressure.

Table 2
Capacitance values ($F g^{-1}$) from galvanostatic cycling at various current for PFA-derived ACs. Voltage window 2.5 V. Current range applied from 0.3 to 225 $A g^{-1}$ (equivalent to 1 to 1000 mA).

Sample	$C_{I(A\ g^{-1})}$ ($F g^{-1}$)				
	$C_{0.3}$	C_{15}	C_{90}	C_{180}	C_{225}
PFA-K1	65	16	[a]	[a]	[a]
PFA-K2	97	81	68	53	[a]
PFA-K2.5	127	112	99	90	87
PFA-K3	147	134	120	109	103
Maxsorb	117	104	87	[a]	[a]
RP-20	100	85	81	80	79
Supra	100	90	84	83	80

[a] Negligible capacitance measurable at high currents.

Ref. [39]). It is worth mentioning however, that samples PFA-K2.5 and PFA-K3 were less affected by increases in current density and could be cycled up to current densities as high as 225 $A g^{-1}$ with only a 30% decrease in their initial capacitance values.

The excellent capacitative behaviour of these samples is demonstrated by their galvanostatic charge–discharge profiles displayed in Fig. 3. For samples PFA-K3 and PFA-K2.5, both the charge and discharge stages are very linear with negligible curvature in their *V* vs. *t* profile at current densities of 7 and 90 $A g^{-1}$ (Fig. 3(a) and (b), respectively). Also, as is typically observed for EDLCs, an increase in current density leads to a more visible IR drop on initial charging or discharging.

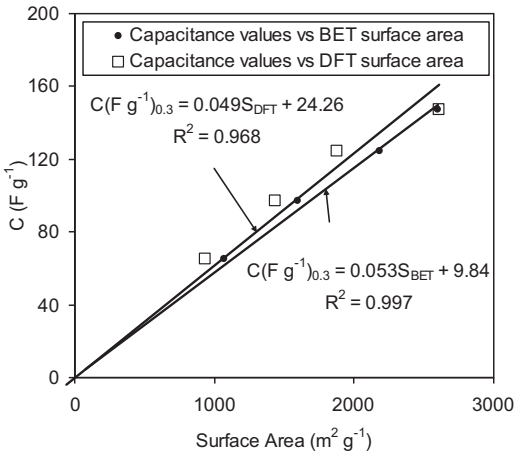

Fig. 4. Specific capacitance values for PFA-derived carbons vs. BET area. Current density 0.3 $A g^{-1}$. Voltage window 0–2.5 V.

The specific capacitance values obtained at a low current density (0.3 $A g^{-1}$), where the ions have sufficient time to enter and diffuse into the porosity of the material, are plotted vs. the surface area in Fig. 4 for the corresponding ACs (both BET and DFT areas). A linear relationship between surface area vs. capacitance is found and this implies that the capacitance values are controlled primarily by the surface area of the active material [40]. It has been reported [40] that such a linear relationship is only true for materials with low surface areas and that for samples with high surfaces areas (≤~1500 $m^2 g^{-1}$ BET (S_{BET}) or ~1200 $m^2 g^{-1}$ DFT (S_{DFT})) the capacitance values begin to level off and exhibit a small plateau [40]. In the work presented by Barbieri et al. [40], the plateau is considered to be independent of the estimation of surface area of the materials, as similar behaviour was found with either BET or DFT models for the calculation of surface area. The authors also discarded accessibility restrictions of the electrolyte ions into the very small pores (below 0.7 nm) as the reason for the presence of the so-called plateau in the representation of capacitance ($F g^{-1}$) vs. S_{BET} (or S_{DFT}). Rather, capacitance saturation on very thin pore walls of high surface area materials was proposed. Therefore, based on the results shown in Fig. 4 it appears plausible to consider that

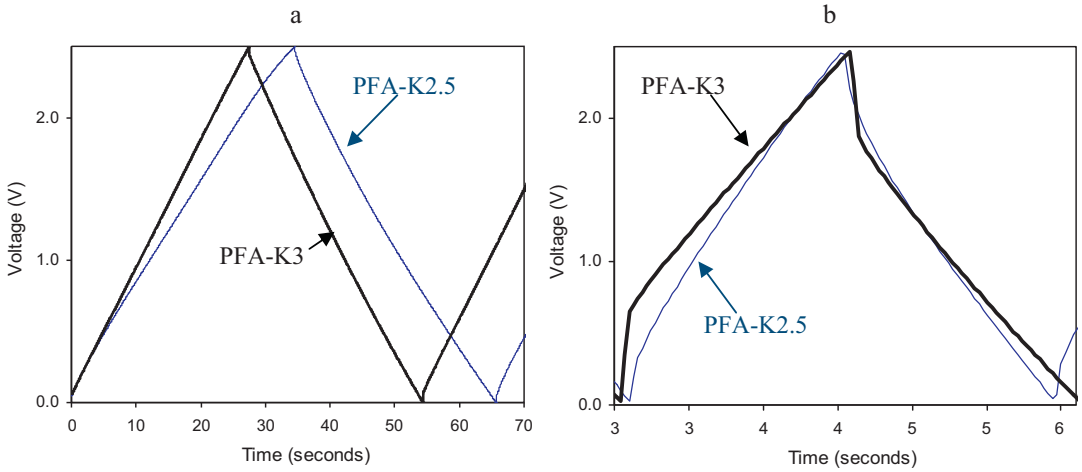

Fig. 3. Galvanostatic charge–discharge profiles for PFA-K3 and PFA-K2.5 samples. Currents applied: (a) 7 and (b) 90 $A g^{-1}$. Voltage window 0–2.5 V.

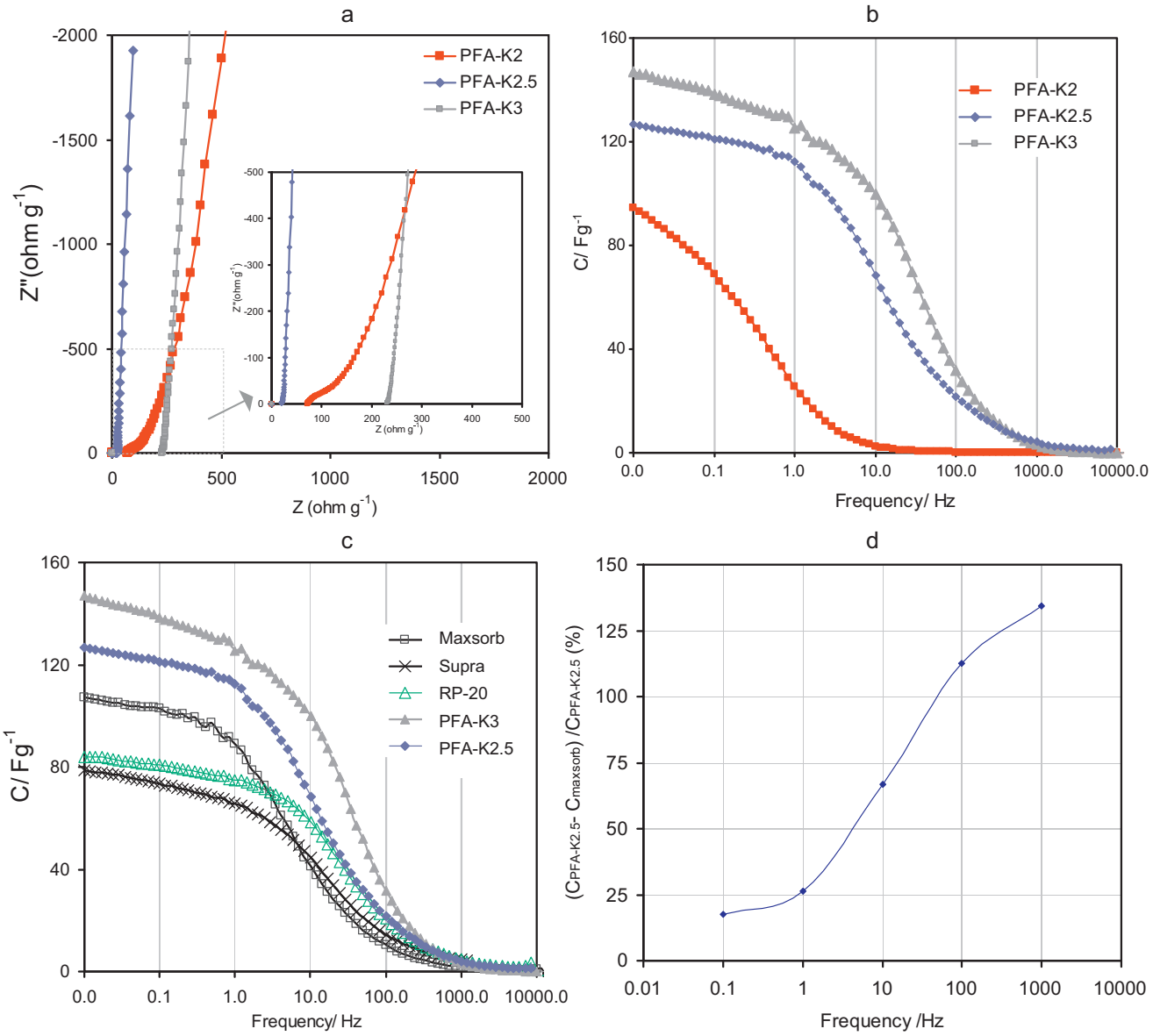

Fig. 5. (a) Impedance spectroscopy spectra for PFA-series (insert: magnification of the high frequency region). (b) Specific capacitance values as function of frequency for PFA-series. (c) Impedance spectroscopy spectra for commercial ACs plotted against PFA-derived ACs. (d) Specific capacitance values from impedance spectra for PFA-K2.5 relative to Maxsorb (%). Frequency range 10 mHz to 100 kHz. Completely discharged state.

the materials developed in the work reported here might have pore walls with sufficient thickness to accommodate a high amount of charge at a given electrode potential.

As can be seen in Fig. 4, the experimental points (capacitance values, $F\,g^{-1}$, and surface area, $m^2\,g^{-1}$) have been fitted to straight lines passing through the origin. It is worth mentioning that the values provided by the BET model present a slightly better correlation ($R^2 = 0.997$) than those given by the DFT model ($R^2 = 0.967$).

Impedance spectroscopy is a powerful method for investigating the penetration of alternating current into the pore system of the electrode material and also provides information on ion access into the pores at a specific frequency. The Nyquist plots obtained for the ACs PFA-K2, K2.5 and K3 are displayed in Fig. 5(a). The impedance values have been normalized to the mass of active material corresponding at each device. All the profiles show the absence of a loop in the high-frequency region and thereby reflects good ion penetration into the porosity of the carbons [41–43].

At low frequencies, the imaginary part increases sharply and a vertical line is observed showing the pure capacitive behaviour of PFA-K2.5 and PFA-K3. The deviation observed for PKA-2 (a small high-frequency arc) is related to ion diffusion issues within the porous electrode network. The relatively small pore size of PFA-K2 ($L_0 = 0.8$ nm, Table 1) is expected to hinder the movement of electrolyte ions within the pores. This observation is consistent with literature reports on Et_4N^+ and ion sizes, i.e., ~0.68–0.74 and ~0.45–0.49 nm diameter for the cation and the anion, respectively, and 1.3 and 1.16 nm if the solvation sphere of the ions is also take into account for the $Et_4N^+ \cdot 7ACN$ and $BF_4^- \cdot 9ACN$ species, respectively [44–48].

Several capacitive models can be applied to EIS data to display the capacitance variation with frequency [49–51]. The general absence of a high-frequency loop, and the close-to-vertical response for samples PKA-K2.5 and PKA-K3 indicates that the specific capacitance values for the carbons investigated in this study can be calculated according to the following relation:

$C = -1/[\omega Z''(f)]$, where f is the frequency (Hz), ω is equal to $2\pi f$, and Z'' is the imaginary part of impedance.

A capacitance vs. frequency plot is shown in Fig. 5(b). The capacitance maximum occurs, as expected, at the lowest frequencies (<0.1 Hz) due to the kinetic dependence of the ion accessibility to the porous network. Nevertheless, samples PFA-K2, PFA-K2.5 and PFA-K3 still contribute a relatively high capacitance value even at 1.0 Hz (33, 68 and 100 F g^{-1}, respectively). The results displayed by sample PFA-K3 are quite remarkable as specific capacitance values of ~30 F g^{-1} can be supplied at a frequency of 100 Hz, where the majority of the other ACs begin to provide negligible capacitance.

The chemical activation of PFA creates an excellent conductive material with a porosity that can be tuned to deliver porous materials with improved electrolyte ion diffusion dynamics and ion accessibility that lead to improved high frequency performance.

3.3. Comparative study with commercial ACs

Three commercial activated carbons, namely, Maxsorb, RP-20 and Supra that are manufactured and distributed as EDLC electrode materials were evaluated and compared with the performance of the PFA carbons. The adsorption isotherms given in Fig. 1(c) indicate that they are predominantly microporous carbons having surface areas ranging from 1742 to 2112 m^2 g^{-1} (Table 1). The specific capacitance values provided by these samples, using identical electrode preparation and cell construction techniques to that of the PFA series carbons, are tabulated in Table 2. At very low current densities (0.3 A g^{-1}), the capacitance values of the commercial carbons are close to 100 F g^{-1}. The Maxsorb carbon, which has a slightly higher surface area, presents capacitance values of well over 100 F g^{-1} at low-to-moderate charge densities, but at current densities greater than 90 A g^{-1} the capacitance of the Maxsorb system could not be measured (or was negligible) due an increased ohmic drop arising from a combination of electronic and ionic resistances within the electrode. Fig. 5(c) plots the capacitance dependence with the frequency for the commercial samples, with the result for PFA-K2.5 and PFA-K3 included for compassion purposes. As can be seen, PFA-derived ACs give higher capacitance values over the frequency range investigated.

In order to make a fair comparison between samples, the electrochemical behaviour of Maxsorb and PFA-K2.5 AC is examined closely as these materials have very similar textural properties. Despite having comparable surface area, average pore size and pore volume in the mesoporous range (see Table 1), their electrochemical performance in Et_4NBF_4/ACN is markedly different. Specific capacitance values obtained from galvanostatic cycling experiments are around 8–14% higher for PFA-K2.5 than in the case of using the commercial sample. More importantly, PFA-derived carbon can be cycled up to a current density of 225 A g^{-1}, whereas Maxsorb could only be cycled up to 90 A g^{-1}. In terms of frequency response, PFA-K2.5 presents a noticeably superior performance than Maxsorb (Fig. 5(c)). Fig. 5(d) shows that at a small frequency (1 Hz) the capacitance of PFA-K2.5 is close to 25% higher than that provided by Maxsorb. This difference becomes more extensive towards higher frequency values. At a frequency of 1 kHz, the PFA-derived material provides a capacitance 125% higher than Maxsorb, demonstrating the better high-frequency performance of the prepared material. One probable explanation for these results can be found in their different electrical resistivity. PFA-K2.5 has a resistivity value of 0.0157 Ω cm whereas Maxsorb's resistivity is 0.0441 Ω cm for the same applied compaction pressure (36 MPa).

4. Conclusions

The electrical double layer capacitance of activated carbons, prepared by KOH activation of polyfurfuryl alcohol in an organic electrolyte, has been determined. This combination of precursor and activation technique provides an ideal electronic and ionic pore structure for electrochemical energy-storage devices (e.g., electrical double-layer capacitors). The porous carbons exhibit high capacitance values (up to 147 F g^{-1}) in 1 M tetraethylammonium tetrafluoroborate, in acetonitrile, at 2.5 V. Due to the desirable combination of high surface area, good electronic conductivity and optimal pore size, an outstanding rate capability is also observed. Capacitance values of up to 100 F g^{-1} at a current density of 225 A g^{-1} are obtained.

In comparison with commercial activated carbons possessing similar textural properties, PFA-derived carbons provide 25% greater capacitance at 1 Hz, increasing to 125% greater capacitance at a frequency of 10 Hz. At 100 Hz, the PFA carbons can deliver >30 F g^{-1}, making these materials very promising for the fabrication of high-frequency supercapacitors.

Acknowledgement

This work was funded through the CSIRO Energy Transformed Flagship.

References

[1] P. Simon, Y. Gogotsi, Nat. Mater. 7 (2008) 845–854.
[2] M. Inagaki, H. Konno, O. Tanaike, J. Power Sources 195 (2010) 7880–7903.
[3] E. Frackowiak, F. Béguin, Carbon 39 (2001) 937–950.
[4] B.E. Conway, Electrochemical Capacitors, Kluwer Academic, New York, 1999.
[5] S. Sarangapani, B.V. Tilak, C.P. Chen, J. Electrochem. Soc. 143 (1996) 3791–3799.
[6] R. Kotz, M. Carlen, Electrochim. Acta 45 (2000) 2483–2498.
[7] H. Shi, Electrochim. Acta 41 (1996) 1633–1639.
[8] A.G. Pandolfo, A.F. Hollenkamp, J. Power Sources 57 (2006) 11–27.
[9] F. Rodriguez-Reinoso, M. Molina-Sabio, Carbon 30 (1992) 1111–1118.
[10] T. Tay, S. Ucar, S. Karagöz, J. Hazard. Mater. 165 (2009) 481–485.
[11] W. Li, K. Yang, J. Peng, L. Zhang, S. Guo, H. Xia, Ind. Crop. Prod. 28 (2008) 190–198.
[12] W.M. Qiao, S.H. Yoon, Y. Korai, I. Mochida, S. Inoue, T. Sakurai, T. Shimohara, Carbon 42 (2004) 1327–1331.
[13] M. Endo, T. Takeda, Y.J. Kim, K. Koshiba, K. Ishii, Carbon Sci. 1 (2001) 117–128.
[14] D. Esrafilzadeh, M. Morshed, H. Tavanai, Synth. Met. 159 (2009) 267–272.
[15] K. Nakagawa, S.R. Mukai, K. Tamura, H. Tamon, Chem. Eng. Res. Des. 85 (2007) 1331–1337.
[16] A. Ahmadpour, D.D. Do, Carbon 34 (1997) 471–479.
[17] T.Y. Zhang, W.P. Walawender, L.T. Fan, M. Fan, D. Daugaard, R.C. Brown, Chem. Eng. J. 105 (2004) 53–59.
[18] H. Marsh, F. Rodríguez-Reinoso, Activated Carbon, Elsevier, London, 2006.
[19] H.E. Hoydonckx, W.M. Van Rhijn, W. Van Rhijn, D.E. De Vos, P.A. Jacobs, Ullmann's Encyclopedia of Industrial Chemistry, 2007, pp. 1–29.
[20] L. Burket, R. Rajagopalan, H.C. Foley, Carbon 45 (2007) 2307–2320.
[21] M. Choura, N.M. Belgacem, A. Gandini, Macromolecules 29 (1996) 3839–3850.
[22] M.M. Dubinin, in: D.A. Cadenhead (Ed.), Progress in Surface and Membrane Science, vol. 9, Academic Press, London, 1975.
[23] H.F. Stoeckli, L. Ballerini, Fuel 70 (1991) 557–559.
[24] A. Espinola, P. Mourente Miguel, M. Roedel Salles, A. Ribeiro Pinto, Carbon 24 (1986) 337–341.
[25] Y.J. Kim, Y. Horie, Y. Matsuzawa, S. Ozaki, M. Endo, M. Dresselhaus, Carbon 42 (2004) 2423–2432.
[26] Z. Shen, R. Xue, Fuel Process. Technol. 84 (2003) 95–103.
[27] S. Mrozowski, Third Biennial Carbon Conference, 1958, pp. 495–508.
[28] J. Sánchez-González, A. Macías-García, M.F. Alexandre-Franco, V. Gómez-Serrano, Carbon 43 (2005) 741–747.
[29] A. Alonso, V. Ruiz, C. Blanco, R. Santamaria, M. Granda, R. Menendez, S.G.E. de Jager, Carbon 44 (2006) 441–446.
[30] R.L. Istvan, The Patent Description & Claims USPTO Patent Application 20090246528.
[31] D. Qu, H. Shi, J. Power Sources 74 (1998) 99–107.
[32] T.-C. Weng, H. Teng, J. Electrochem. Soc. 148 (4) (2001) A368–A373.
[33] D. Zhai, H. Du, B. Li, Y. Zhu, F. Kang, Carbon 49 (2011) 718–736.
[34] Y.-B. Xie, W.-M. Qiao, W.-Y. Zhang, G.-W. Sun, L.-C. Ling, Carbon 49 (2011) 352–355.
[35] S.S. Barton, J.E. Koresh, Carbon 22 (1984) 481.
[36] S. Biniak, A. Swiatkowski, M. Pakula, L.R. Radovic (Eds.), Chemistry and Physics of Carbon, vol. 27, Marcel Dekker, New York, 2001, p. 125.

[37] K. Kierzek, E. Frackowiak, G. Lota, G. Grygle Wicz, J. Machnikowski, Electrochim. Acta 49 (2004) 515–523.
[38] A.G. Pandolfo, G.J. Wilson, T.D. Huynh, A.F. Hollenkamp, Fuel Cells 10 (2010) 856–864.
[39] V. Ruiz, A.G. Pandolfo, Electrochim. Acta 55 (2010) 7495–7500.
[40] O. Barbieri, M. Hahn, A. Herzog, R. Kotz, Carbon 43 (2005) 1303–1310.
[41] C.L. Liu, W.S. Dong, G.P. Cao, J.R. Song, L. Liu, Y.S. Yang, J. Electrochem. Soc. 155 (2008) F1–F7.
[42] M. Toupin, D. Belanger, I.R. Hill, D. Quinn, J. Power Sources 140 (2005) 203–210.
[43] C. Portet, P.L. Taberna, P. Simon, C. Laberty-Robert, Electrochim. Acta 49 (2004) 905–912.
[44] M. Ue, K. Ida, S. Mori, J. Electrochem. Soc. 141 (1994) 2989.
[45] M. Endo, Y.J. Kim, H. Ohta, K. Ishii, T. Inoue, T. Hayashi, Y. Nishimura, T. Maeda, M.S. Dresselhaus, Carbon 40 (2002) 2613–2626.
[46] R. Lin, P.L. Taberna, J. Chimiola, D. Guay, Y. Gogotsi, P. Simon, J. Electrochem. Soc. 156 (2009) A7–A12.
[47] J. Segalini, B. Daffos, P.L. Taberna, Y. Gogotsi, P. Simon, Electrochim. Acta 55 (2010) 7489–7494.
[48] C.M. Yang, Y.-J. Kim, M. Endo, H. Kanoh, M. Yudasaka, S. Ijima, K. Kaneko, J. Am. Chem. Soc. 129 (2007) 20.
[49] J.F. Fauvarque, P. Simon, in: F. Beguin, E. Frackowiak (Eds.), Carbons for Electrochemical Energy Storage and Conversion Systems, 2010, p. 31.
[50] F. Rafik, H. Gualous, R. Gallay, A. Crausaz, A. Berthon, J. Power Sources 165 (2007) 928–934.
[51] C. Portet, G. Yushin, Y. Gogotsi, J. Electrochem. Soc. 155 (2008) A531–A536.